Liquid Crystals
Publication details, including instructions for authors and subscription information:
http://www.informaworld.com/smpp/title~content=t713926090

Evidence for lateral chain conformation change in the solid phase of substituted nematogens

F. Perez[a]; P. Judeinstein[a]; J. P. Bayle[a]; H. Allouchi[b]; M. Cotrait[b]; E. Lafontaine[c]
[a] Laboratoire de Chimie Structurale Organique, Université Paris XI, ORSAY Cedex, France [b] Laboratoire de Cristallographie et Physique Cristalline, Université Bordeaux I, Talence Cedex, France [c] DGA/CREA, Arcueil Cedex, France

To cite this Article Perez, F. , Judeinstein, P. , Bayle, J. P. , Allouchi, H. , Cotrait, M. and Lafontaine, E.(1996) 'Evidence for lateral chain conformation change in the solid phase of substituted nematogens', Liquid Crystals, 21: 6, 855 — 864
To link to this Article: DOI: 10.1080/02678299608032902
URL: http://dx.doi.org/10.1080/02678299608032902

LIQUID CRYSTALS, 1996, VOL. 21, NO. 6, 855–864

Evidence for lateral chain conformation change in the solid phase of substituted nematogens

by F. PEREZ, P. JUDEINSTEIN, J. P. BAYLE*
Laboratoire de Chimie Structurale Organique, URA 1384 CNRS Bât. 410,
Université Paris XI, 91405 ORSAY Cedex, France

H. ALLOUCHI, M. COTRAIT
Laboratoire de Cristallographie et Physique Cristalline, ERS 133 CNRS 351,
Cours de la Libération, Université Bordeaux I, 33405 Talence Cedex, France

and E. LAFONTAINE
DGA/CREA, 16 bis Avenue Prieur de la Côte d'Or, 91414 Arcueil Cedex, France

(*Received 20 May 1996; in final form 18 July 1996*)

A new homologous series of 4-(4-chlorobenzoyloxy)-2-alkoxy-3-methyl-4′-(4-*trans*-pentylcyclohexanoyloxy)azobenzenes has been synthesized. These compounds contain four rings in the main core, a lateral alkoxy branch and an adjacent lateral methyl group on one inner ring. They present a large nematic range and a solid–solid phase transition for the first members of the series. The crystal structures of two similar compounds containing a lateral butoxy chain have been solved. The HM4 compound ($C_{31}H_{33}N_2O_5Cl$) is derived from the series, but does not have the terminal pentyl chain while the PM4 compound ($C_{36}H_{43}N_2O_5Cl$) possesses this terminal chain. HM4 and PM4 crystallize, respectively, in $P2_1/c$ ($Z=4$) and $P\bar{1}$ ($Z=2$) space groups. The final reliability factors are $R=0{\cdot}138$ for HM4 (the terminal cyclohexyl ring is largely disordered) and $R=0{\cdot}041$ for PM4, for 2204 and 1963 observed reflections, respectively. The four ring central core is linear and rigid for both compounds. The conformation of the butyloxy side chain branched on one of the central phenyl rings is very dependent on the terminal substituent, as it is found in a largely bent conformation in HM4 and in an extended conformation in PM4. To monitor the lateral chain conformation in the solid and nematic phase, we have used the $-OCH_2-$ resonance in the ^{13}C MAS NMR spectra. The temperature dependence of this resonance has indicated that the solid–solid transition encountered for the first members of the series is associated with a change of the lateral chain conformation within the solid phase. At the solid–nematic transition, the change of the chain conformation involving the first segment of the lateral chain is far less pronounced. When this solid–solid phase transition disappears for the last members of the series, this change in the conformation occurs at the solid–nematic transition.

1. Introduction

We have shown recently that laterally alkoxy-substituted compounds can have a large enantiotropic nematic range when the mesogenic core contains four rings and when the lateral chain is introduced on one of the inner rings [1–3]. The crystal structure of one of these compounds indicated that the molecule was roughly planar, the terminal and the lateral chains being in the same plane. The conformation of the lateral chain was found to be all-*trans* and its orientation *quasi*-perpendicular to chains belonging to the main core [3]. The DSC and ^{13}C MAS NMR spectra of the compounds show that the conformation for the first carbons within the lateral chain does not evolve in the solid phase. On the contrary, at the solid–nematic transition, a conformation change occurs for the lateral chain. As a consequence, in the nematic phase, the lateral flexible substituent adopts a special conformation and is more or less oriented along the molecular long axis [4–9]. The lateral chain conformation in the solid and nematic phase may be influenced by any nearby substituent which can sterically hinder the all-*trans*-conformation of the chain in the solid phase and partially bend the lateral chain along the mesogenic core. Following this concept, we present in this paper the synthesis of some new laterally substituted compounds in which a lateral

*Author for correspondence.

methyl group is introduced into the *ortho*-position to the lateral alkoxy chain. The chain conformation in the solid phase is obtained through the X-ray structures of two homologous compounds in which the terminal group is a hydrogen or an *n*-pentyl chain. Then, in order to follow unambiguously the conformation of the lateral $-OCH_2-$ fragment, ^{13}C MAS NMR is used to study both the solid and the nematic phases.

2. Experimental

2.1. *Synthesis*

The compounds were prepared according to the synthetic scheme shown below:

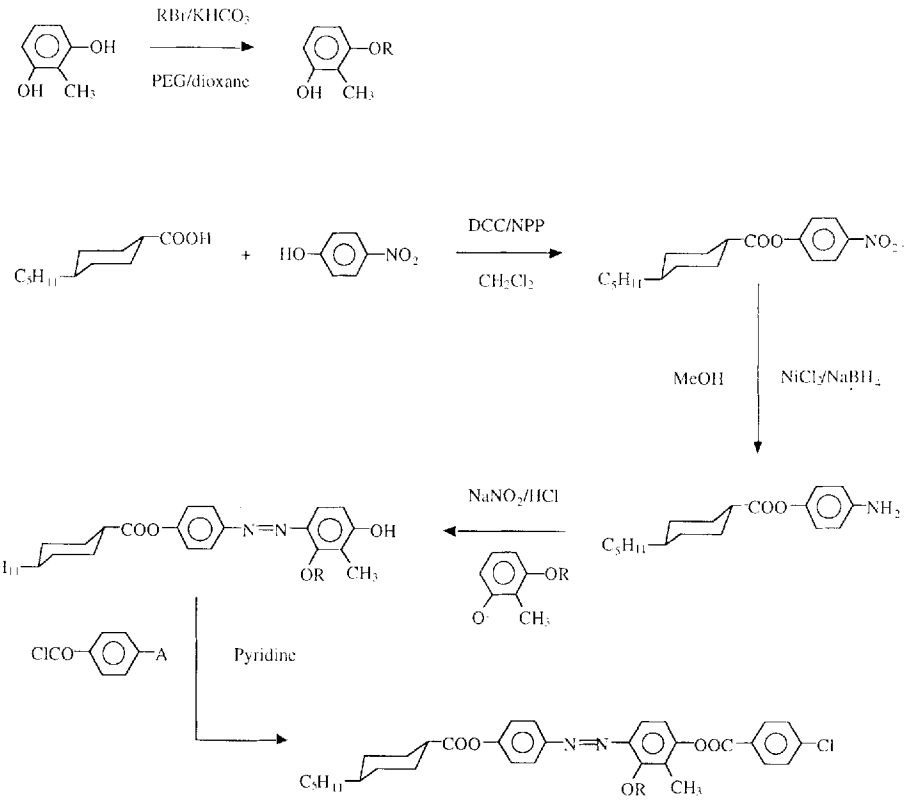

4-*trans*-*n*-Pentylcyclohexane-l-carboxylic or cyclohexanecarboxylic acid was esterified with 4-nitrophenol using the DCC method [10]. Then, the nitro group was selectively reduced in methanol using $NiCl_2$ and $NaBH_4$ [11]. The crude amine was diazotized in a mixture of PEG/dioxane/water (25/70/5); (PEG = polyethylene glycol, MW = 200). Then, the diazonium salt was coupled with 3-alkoxy-2-methylphenol which was obtained from 2-methylresorcinol by monoetherification using PEG/dioxane (25/75) as solvent [12]. The diazo-coupling reaction occurs mainly in the *para*-position to the hydroxy group and therefore in the *ortho*-position to the alkoxy chain, as shown by carbon–carbon connectivity NMR experiments and X-ray diffraction studies for an analogous compound [13]. The crude compound was chromatographed on silica gel (60–200 mesh). Using chloroform as eluent, the compound was collected as the last fraction. Then, the compound was recrystallized from hexane.

The fourth ring was introduced by esterification in dry pyridine using 4-chlorobenzoyl chloride at room temperature in order to avoid *trans*-esterification. The final compound was chromatographed on silica gel (60–200 mesh), and the first fraction collected using chloroform as eluent. The esters were recrystallized from $CHCl_3/CH_3CN$ and $CHCl_3/C_2H_5OH$ mixtures (80/20) until constant transition temperatures were obtained. The structures and the purities of the compounds were checked using ^1H NMR (AM 250 Bruker spectrometer) and by mass spectrometry (R10-10C Nermag mass spectrometer). In the text, the compounds are labelled by the number (*n*) of carbons in the lateral alkoxy chain as PM*n* and HM*n*, indicating whether the compounds have or do not have the terminal pentyl chain.

2.2. *DSC measurements*

The phase transitions were observed and characterized by using an Olympus polarizing microscope, fitted with an FP 82 Mettler heating stage, and an FP 85 Mettler

DSC. Scans were recorded without prior melting of the samples, and all transition temperatures (see tables 1 (*a*) and 1 (*b*)) were obtained at a 10°C min^{-1} heating rate.

2.3. *X-ray data collection and structure resolution*

Suitable crystals of PM4 and HM4 were grown from $CHCl_3/CH_3CN$ solution at 293 K. The cell parameters were obtained and data collection made with a CAD-4 Enraf-Nonius diffractometer, equipped with a graphite monochromator. The crystal data, the data collection and the refinement characteristics are given in table 2. Both structures were solved by direct methods, using the Shelx86 package [14] for HM4 and the Mithril package [15] for PM4; the positions of two thirds of the non-hydrogen atoms for HM4 and of almost all the non-hydrogen atoms for PM4 were obtained, and the remaining atoms were located after successive Fourier syntheses. Atomic parameters were refined isotropically, then anisotropically, under constraints with the Shelx76 package [14] for HM4, and without constraints with the local Crisaf program for PM4. Hydrogen atoms were introduced in theoretical positions [16] and allowed to ride with the atoms to which they were attached. The atomic scattering factors were taken from the International Tables for X-ray Crystallography (1974, Vol. IV). The final reliability factors were $R=0{\cdot}138$ and $R_w=0{\cdot}159$ for HM4, and $R=0{\cdot}041$ and $R_w=0{\cdot}043$ for PM4. The poor reliability factor for HM4 is due to the very high thermal motion and some disorder of the cyclohexyl ring.

Table 1 (*a*). Transition temperatures in (°C) for the 4-(4-chlorobenzoyloxy) - 2 - alkoxy - 3 - methyl - 4′ - (4 - *trans*-pentylcyclohexanoyloxy)azobenzenes series (PM*n*). The DSC heating rate was 10°C min^{-1}.

n	Cr_1	→	Cr_2	→	S	→	N	→	I
4	•	95	•		—	112	•	237·5	•
6	•	75	•		—	94	•	215	•
8	•	66·5	•		—	84	•	198	•
10	•	73	•		—	80·5	•	190·5	•
12	—		—		•	73·5	•	177·5	•
14	—		—		•	77	•	167·5	•
16	—		•	65	•	82	•	157	•

Table 1 (*b*). Melting temperatures (in °C) for 4-(4-chlorobenzoyloxy)-2-alkoxy-3-methyl-4′-(cyclohexanoyloxy)-azobenzenes (HM*n*). The DSC heating rate was 10°C min^{-1}.

n	Cr	→	I
4	•	147	•
14	•	88	•

2.4. *^{13}C NMR spectra in the solid and nematic phase*

High resolution ^{13}C NMR experiments were performed using a Bruker MSL 200 spectrometer with quadrature detection and with a double-tuned coil for ^{13}C and ^{1}H NMR. The crystalline samples were filled into fused zirconia rotors fitted with boron nitride caps and spun at 6 kHz at the magic angle (54·7°). ^{13}C chemical shifts were referenced to the glycine carbonyl signal (assigned at 176·03 ppm), used as external reference. The spectra were obtained using a cross-polarization pulse (with a ^{1}H 90° pulse of 4·1 μs), high power decoupling during acquisition, 0·03 s acquisition time, 3 s recycle delay, 512 scans and 1·2 ms mixing time. Variable temperature CP/MAS NMR experiments were performed in the 30–150°C range using a EUROTHERM temperature controller, calibrated with DABCO (1,4-diazabicyclo[2.2.2]octane); crystal–crystal transition [17].

3. Results and discussion

3.1. *DSC measurements*

The transition temperatures of the PM*n* compounds are given in table 1 (*a*). All compounds form enantiotropic nematic phases with large liquid crystalline ranges. Figure 1 shows the dependence of the transition temperatures on the number of atoms (*n*) in the lateral alkoxy chain. The decrease in T_{NI} (Nematic–Isotropic transition temperature) is rather smooth and the T_{CrN} evolution (Crystal–Nematic transition) is flat, as already observed for similar series containing a single lateral chain. The presence of the flexible and the rigid substituent on the same side of the inner alkoxy substituted aromatic ring does not perturb the nematic phase to a large extent. The effect is similar to that observed for conventional mesogens with rigid substituents. When a lateral methyl group is introduced next to a second methyl group, an enhancement of the nematic–isotropic transition and an increase of the thermal stability of the mesophase are observed [18,19], due to the fact that the second substituent fills the empty space generated by the first. Similarly, in our compounds, the methyl group can accommodate the free space created by the lateral chain folded back along the mesogenic core in the nematic phase. A solid–solid transition is observed for the first four members of the series. Two DSC curves for PM4 are presented in figure 2. The solid–solid phase transition (figure 2 (*a*)) disappears if the DSC curve is recorded after heating the sample above the solid–solid transition or above the solid–nematic transition (figure 2 (*b*)), followed by cooling. If the sample is crystallized quickly by decreasing the chloroform percentage in the solvent mixture, this solid–solid phase transition can disappear and the DSC curve is similar to that displayed in figure 2 (*b*).

Table 2. Crystal data, data collection and refinement characteristics for HM4 and PM4.

Parameter	HM4	PM4
Data collection		
chemical formula	$C_{31}H_{33}N_2O_5Cl$	$C_{36}H_{43}N_2O_5Cl$
molecular weight (g mol^{-1})	549·1	619·2
crystal system	monoclinic	triclinic
space group	$P2_1/c$	$P\bar{1}$
a (Å)	24·852(3)	12·615(9)
b (Å)	13·360(1)	12·93(1)
c (Å)	7·118(1)	13·703(9)
α (°)	90·00	95·43(8)
β (°)	92·63(1)	113·69(6)
γ (°)	90·00	117·96(6)
volume of cell (Å^3)	2891	1693
no. of molecules per unit cell (Z)	4	2
radiation	CuKα	MoKα
wavelength (Å)	1·54178	0·71073
density (g cm^{-3})	1·262	1·214
number of reflections for cell parameters	25	19
θ range (°)	25–31	0–13
absorption μ (mm^{-1})	1·515	0·161
crystal shape	prism	prism
crystal colour	red	red
temperature (K)	293	293
h_{min}, h_{max}	0, 26	0, 15
k_{min}, k_{max}	−17, 17	−15, 15
l_{min}, l_{max}	−7, 7	−16, 16
scan	ω–2θ	ω–2θ
measured reflections	7967	3118
independent reflections	3646	2291
observed reflections	2204	1963
criterion for observed $I > n\sigma(I)$	3	3
θmax (°)	55	25
standard reflections	3	3
Refinement		
refinement	on F	on F
reliability factor	0·138	0·041
R_w	0·159	0·043
weight w	$1/(\sigma(F)^2+0{\cdot}055F^2)$	$1/\sigma(F)^2$
number of refined parameters	351	569

3.2. *X-ray analysis*

The fractional coordinates and the equivalent U_{eq}(Å^2) factors for HM4 and B_{eq}(Å^2) for PM4 are given in tables 3(*a*) and 3(*b*). The thermal U_{eq}(Å^2) factors are very high for the atoms of the terminal cyclohexane carboxylate group in HM4. This is illustrated by the SNOOPI [20] drawing of this molecule presented in figure 3(*a*). This gives very imprecise values of bond lengths and angles, characterized by high standard deviations. In PM4, the terminal pentyl chain considerably reduces the thermal motion of the cyclohexane ring (figure 3(*b*)). The stick-and-ball molecular representation and the atom labelling of non-hydrogen atoms are presented in figures 4(*a*) and 4(*b*), respectively for HM4 and PM4. As expected, the steric interaction between the methyl group and the side-chain clearly modifies the chain orientation, as the latter is tilted from the perpendicular orientation with respect to the main core found in a homologous series of non-methylated compounds [3]. But, surprisingly, the absence of the terminal pentyl chain influences to a large extent the side chain conformation.

The three phenyl rings, designated Φ_1 (atoms C10 to C15), Φ_2 (atoms C20 to C25), and Φ_3 (atoms C30 to C35), are perfectly planar as is the case for the C13–N16=N17–C20 central group; the Φ_1–N=N–Φ_2 group and the terminal *para*-chlorobenzoate group are roughly planar. The cyclohexyl group (atoms C1 to C6) is in the chair conformation in both HM4 and PM4. The terminal pentyl chain in PM4 (atoms C42 to C46) is fully extended. The two groups bonded to the laterally substituted aromatic ring are nearly in a *cis*-position with respect to one another. The molecular

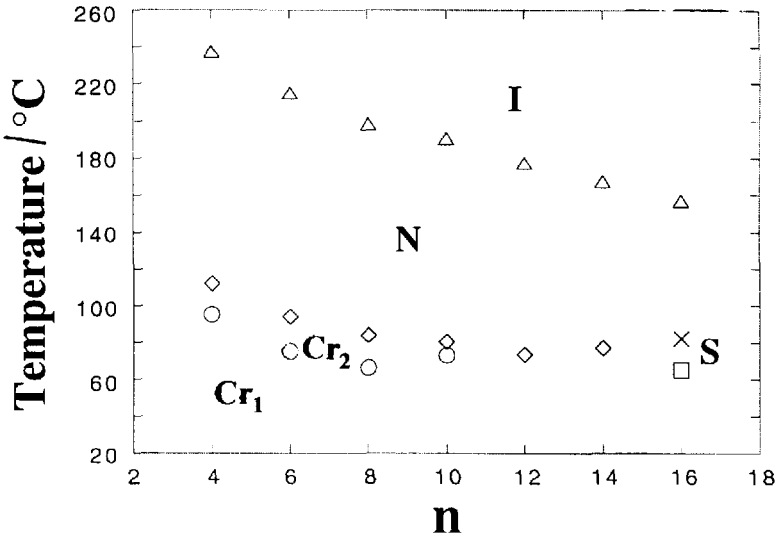

Figure 1. Phase behaviour for the homologous PM*n* series. *n* is the number of carbons in the lateral chain.

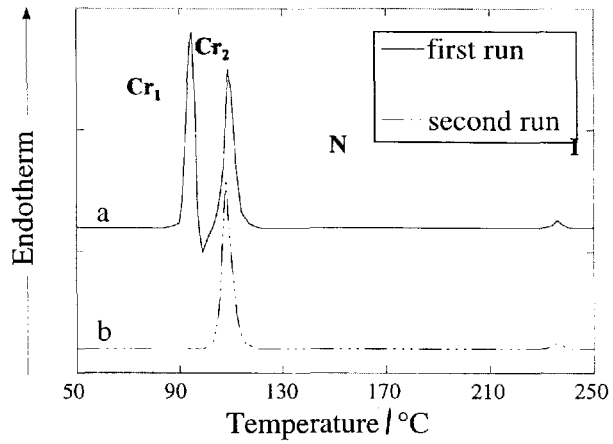

Figure 2. DSC traces for PM4 from room temperature to the clearing temperature: (*a*) with no prior heating; (*b*) with prior heating into the nematic phase at 120°C.

conformations are entirely defined by the significant torsion angles given in table 4. They show that the molecules HM4 and PM4 have completely different polyaromatic core conformations. This is confirmed by the very different angles between the Φ_1, Φ_2 and Φ_3 mean planes: $\Phi_2/\Phi_1 = 45{\cdot}6(5)°$ for HM4 and $9{\cdot}8(3)°$ for PM4, $\Phi_3/\Phi_1 = 10{\cdot}7(5)°$ for HM4 and $62{\cdot}1(5)°$ for PM4 and $\Phi_3/\Phi_2 = 55{\cdot}9(4)°$ for HM4 and $53{\cdot}0(3)°$ for PM4. Nevertheless, the polyaromatic cores of molecules HM4 and PM4 are quite linear with a total length (C1 ... C129) for HM4 equal to 23·30(4) Å and (C46 ... C129) for PM4 equal to 29·81(1) Å. This is corroborated by the value of the C1 ... N16 ... C129 and C46 ... N16 ... C129 angles, respectively equal to $177{\cdot}1(1)°$ and $178{\cdot}(1)°$ for HM4 and PM4. In PM4, the molecules are antiparallel through the centres of symmetry of the $P\bar{1}$ space group. The projection of the structure along the *a* axis is presented in figure 5. The molecular arrangement is typical of a nematogenic compound. The crystal cohesion is probably adopted as a result of dipolar interactions between polar COO groups and very weak Van der Waals interactions between neighbouring molecules. The butyloxy side chain (atoms C36 to C40) is roughly linear for PM4, as is the case for a similar compound in the solid state [17]; the angle between this chain and the polyaromatic core is $147{\cdot}7(1)°$. On the contrary, the alkoxy chain in HM4 has a folded *tgg* conformation, starting to fold back along the polyaromatic main core, in agreement with the conformation in the nematic phase [18–20]. Thus, the reason for the difference in the side chain conformation occurring in HM4 and PM4 is of interest. For large side chains, we can expect that the terminal part of the side chain is able to interact with the central core of a nearby molecule within the crystal. This is not the case in structure HM4, where the butyloxy side chain is too short to give such interactions. In consequence, there should be no great difference in energy between the folded side chain in HM4 and the extended one in PM4, and this energy difference may be overcome by some favourable intermolecular van der Waals contacts.

3.3. ^{13}C *NMR spectra in the solid and nematic phase*

Recently, we have shown with compounds having a single lateral chain, that it is possible to probe the lateral chain conformation by using the –OCH2– ^{13}C resonance in the solid and nematic phases. In that series, a downfield jump is observed when the lateral chain conformation changes from an all-*trans*-conformation in the solid phase to a *gauche*-conformation involving the first

Table 3 (*a*). HM4 fractional coordinates ($\times 10^4$) and equivalent thermal parameters Ueq ($Å^2$) ($\times 10^3$), where Ueq = $(1/3)\ \Sigma_i\ \Sigma_j\ U_{ij}\ \mathbf{a}_i^*\mathbf{a}_j^*\mathbf{a}_i \times \mathbf{a}_j$.

Atom	*x/a*	*y/b*	*z/c*	U_{eq}
C1	16377(15)	1153(24)	1106(47)	276(99)
C2	15900(13)	1338(28)	−243(51)	231(77)
C3	15429(13)	1541(20)	954(46)	221(62)
C4	15270(10)	1102(23)	2712(47)	315(99)
C5	15790(12)	856(23)	3816(41)	208(61)
C6	16198(11)	496(19)	2496(40)	208(60)
C7	14823(10)	1309(34)	3778(35)	263(90)
O8	14419(5)	1465(13)	2382(24)	180(29)
O9	14748(14)	1377(32)	5433(36)	822(99)
C10	13898(7)	1595(17)	2888(28)	129(33)
C11	13584(7)	848(17)	2921(33)	138(31)
C12	13048(6)	1000(13)	3402(26)	106(23)
C13	12817(5)	1758(10)	3483(20)	76(14)
C14	13150(6)	2414(11)	3335(26)	97(19)
C15	13685(6)	2364(15)	2974(28)	116(26)
N16	12276(4)	1916(6)	3828(11)	54(9)
N17	11969(4)	1307(6)	3399(11)	52(9)
C20	11434(4)	1419(6)	3892(12)	40(8)
C21	11055(4)	946(6)	3014(13)	43(9)
C22	10503(4)	968(6)	3414(14)	43(9)
C23	10373(5)	1508(6)	4833(15)	51(10)
C24	10754(4)	1988(6)	5846(13)	46(9)
C25	11276(4)	1948(6)	5344(13)	47(9)
O26	9829(3)	1482(4)	5307(10)	51(6)
C27	9530(4)	2164(6)	5143(13)	45(9)
O28	9709(4)	2818(5)	4693(12)	68(9)
Cl29	7207(2)	1597(3)	6467(7)	109(5)
C30	8963(5)	2022(7)	5558(14)	53(10)
C31	8784(5)	1231(6)	5925(15)	52(10)
C32	8219(5)	1093(9)	6114(19)	72(14)
C33	7894(5)	1754(11)	6093(15)	69(14)
C34	8066(6)	2551(9)	5757(17)	72(14)
C35	8593(6)	2668(8)	5397(17)	68(13)
O36	11203(3)	411(4)	1641(8)	43(6)
C37	11185(6)	763(7)	−269(13)	56(11)
C38	11403(5)	115(8)	−1567(13)	60(12)
C39	12000(7)	−126(11)	−1181(19)	89(18)
C40	12365(8)	573(15)	−1662(32)	130(29)
C41	10093(5)	450(7)	2377(14)	52(10)

Table 3 (*b*). PM4 fractional coordinates and equivalent thermal parameters B_{eq} ($Å^2$), where $B_{eq} = (4/3)\ \Sigma_i\ \Sigma_j\ \beta_{ij}\ \mathbf{a}_i \times \mathbf{a}_j$.

Atom	*x/a*	*y/b*	*z/c*	B_{eq}
C1	0·4137(6)	−0·3175(4)	−1·5038(4)	4·1(3)
C2	0·4975(6)	−0·3661(5)	−1·4352(4)	4·3(3)
C3	0·5871(6)	−0·2885(5)	−1·3070(4)	4·3(3)
C4	0·4955(6)	−0·2866(4)	−1·2627(4)	3·8(2)
C5	0·4146(6)	−0·2338(5)	−1·3286(4)	4·8(3)
C6	0·3253(6)	−0·3128(5)	−1·4556(4)	5·1(3)
C7	0·5802(6)	−0·2105(5)	−1·1365(4)	4·7(3)
O8	0·4950(4)	−0·2437(4)	−1·0926(3)	5·3(2)
O9	0·7004(4)	−0·1319(4)	−1·0826(3)	5·9(2)
C10	0·5460(5)	−0·1803(5)	−0·9776(4)	3·9(3)
C11	0·6590(6)	−0·1714(5)	−0·8901(4)	4·6(3)
C12	0·6960(6)	−0·1198(5)	−0·7791(4)	4·0(2)
C13	0·6193(5)	−0·0810(5)	−0·7598(4)	3·8(2)
C14	0·5085(6)	−0·0885(6)	−0·8486(4)	5·1(3)
C15	0·4706(6)	−0·1387(6)	−0·9598(4)	5·2(3)
N16	0·6410(5)	−0·0335(4)	−0·6483(3)	4·2(2)
N17	0·7314(4)	−0·0407(4)	−0·5702(3)	3·8(2)
C20	0·7485(5)	0·0045(4)	−0·4606(4)	3·5(2)
C21	0·8425(5)	−0·0074(4)	−0·3697(4)	3·6(2)
C22	0·8701(5)	0·0360(4)	−0·2581(4)	3·6(2)
C23	0·7998(6)	0·0857(4)	−0·2462(4)	3·8(2)
C24	0·7031(6)	0·0955(5)	−0·3354(4)	3·9(2)
C25	0·6782(6)	0·0530(5)	−0·4431(4)	4·0(2)
O26	0·8188(4)	0·1226(3)	−0·1368(3)	4·1(2)
C27	0·8767(6)	0·2444(4)	−0·0843(4)	4·1(2)
O28	0·9115(5)	0·3210(3)	−0·1263(3)	6·1(2)
Cl29	0·9381(2)	0·3626(2)	0·3743(1)	6·1(1)
C30	0·8895(5)	0·2678(4)	0·0300(4)	3·7(2)
C31	0·8695(6)	0·1789(5)	0·0822(4)	4·2(3)
C32	0·8839(6)	0·2082(5)	0·1888(4)	4·3(3)
C33	0·9189(6)	0·3247(5)	0·2398(4)	4·8(3)
C34	0·9364(6)	0·4129(5)	0·1878(4)	4·7(3)
C35	0·9222(6)	0·3832(5)	0·0823(4)	4·2(2)
O36	0·9178(4)	−0·0516(3)	−0·3816(3)	4·5(2)
C37	0·8396(6)	−0·1804(5)	−0·4536(4)	4·5(3)
C38	0·9081(6)	−0·1919(5)	−0·5175(4)	4·1(2)
C39	0·8192(7)	−0·3213(5)	−0·6085(5)	5·7(3)
C40	0·8906(8)	−0·3346(6)	−0·6717(5)	7·4(4)
C41	0·9695(6)	0·0248(5)	−0·1587(4)	4·6(3)
C42	0·3197(6)	−0·3994(5)	−1·6321(4)	5·0(3)
C43	0·4000(6)	−0·3936(5)	−1·6916(4)	5·0(3)
C44	0·3058(7)	−0·4730(6)	−1·8176(4)	5·5(3)
C45	0·3850(8)	−0·4733(6)	−1·8761(5)	6·9(4)
C46	0·3005(9)	−0·5506(8)	−1·9975(6)	8·8(5)

carbon fragment. In that series, the conformation change occurred at the solid–nematic transition. In this new series, the same phenomenon is observed, but occurs now for the first members at the solid–solid transition. The MAS NMR spectra of PM6 below, at and above the solid–solid transition are presented in figure 6. The MAS spectra have been obtained without any prior melting of the sample.

In the OCH_2 region, the downfield jump is quite obvious at the solid–solid transition. Amazingly, HM4 and PM4 exhibit completely opposite behaviours for the evolution in the $-OCH_2-$ chemical shift in the solid phase. For the sake of clarity, figure 7 gives the evolution of the chemical shift versus temperature only for the $-OCH_2-$ carbons in HM4, HM14, PM4 and a second PM4 sample obtained by a different crystallization procedure. The isotropic chemical shift is the same for the two series, but slightly depends on the side chain length (76·40 ppm for C4 and 76·73 ppm for C14); the dashed line in figure 7 gives the isotropic $-OCH_2-$ for the C4 chain. For the monotropic compound HM4, a continuous downfield change is shown for the resonance in the solid phase, and no such jump occurs at the clearing temperature. This indicates that the conformation is changing slowly with temperature. For the monotropic

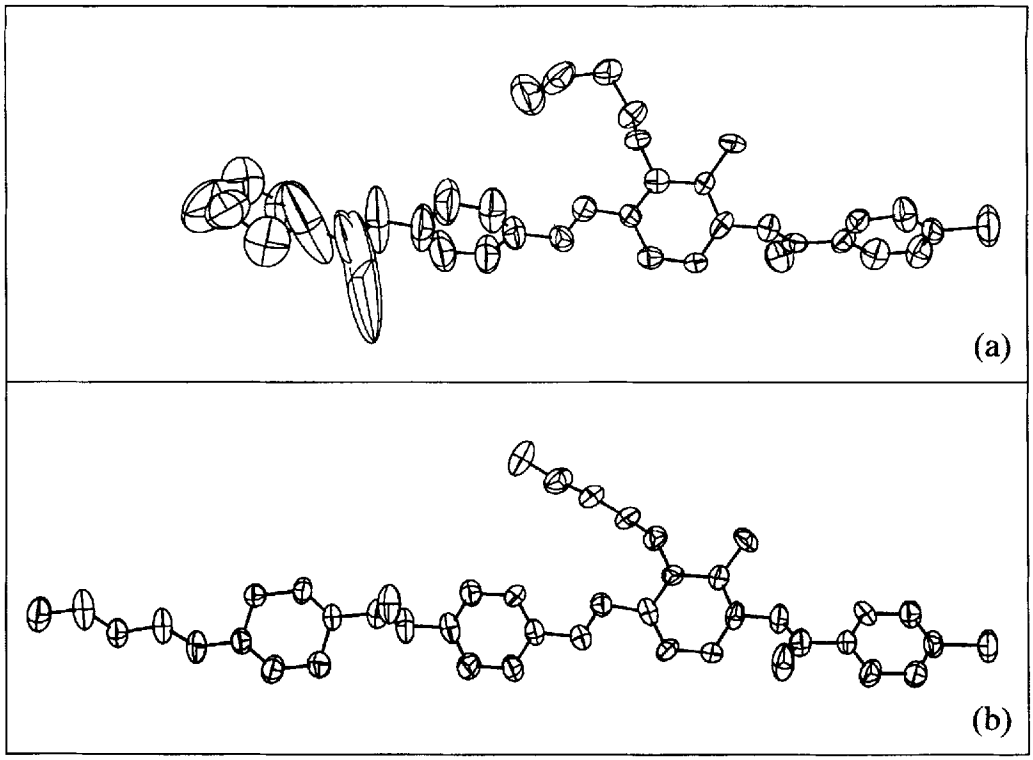

Figure 3. SNOOPI drawing of the molecule HM4 (*a*) and PM4 (*b*). Displacement ellipsoids are drawn at the 50% probability level.

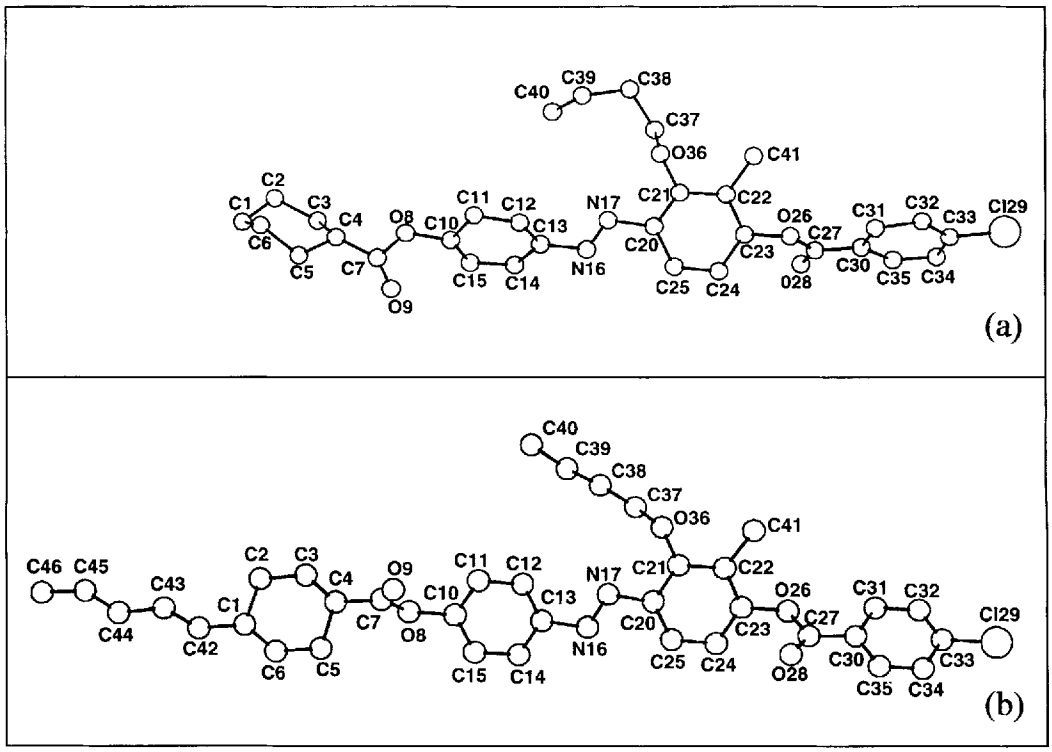

Figure 4. Stick-and-ball representation of the molecule HM4 (*a*) and PM4 (*b*) including the atom labelling.

Table 4. Significant torsion angles in degrees (differing by more 10° from the *trans*-conformation)

Torsion angle	HM4	PM4
C2–C1–C42–C43	—	−66·8(7)
C3–C4–C7–O8	43(3)	−159·9(6)
C7–C8–C10–C11	−91(2)	−55·5(7)
C14–C13–N16–N17	161(1)	*trans*
C20–C21–O36–C37	−90(1)	−64·9(7)
C21–O36–C37–C38	*trans*	143·3(6)
C22–C23–O26–C27	−121(1)	117·3(7)
O36–C37–C38–C39	−64(1)	*trans*
C37–C38–C39–C40	−69(1)	*trans*

compound HM14, this thermal behaviour is negligible, which is certainly a consequence of the chain length. On the contrary, the enantiotropic nematic PM4 exhibits different behaviours at the solid–solid and solid–nematic transitions. A large downfield jump is observed at the solid–solid phase transition, and then at the solid–nematic transition a small upfield shift is encountered. We can conclude that the change in the chain conformation is occurring in the solid phase at the solid–solid phase transition. The role of the solid–solid phase transition in the side chain conformation change is supported by evidence from the second PM4 sample. The chemical shift of the OCH_2 resonance exhibits no discontinuity in the solid phase and slightly decreases to overlap the chemical shift of the first sample near the T_{NI} temperature. Thus, PM4 can be obtained with two different side chain conformations, one extended and the second one folded.

The evolution of the chemical shift for some compounds within the series is presented in figure 8. It is obvious from the plot that, when the solid–solid transition exists, the downfield shift is observed. This happens when the chain is short, leading to weak intermolecular interactions between the side chain and the cores of nearby molecules. Usually, in mesogens bearing a terminal alkoxy chain, all aliphatic carbons show a downfield shift from solution to the solid phase [21–25]. These chemical shift differences are interpreted on the basis of *γ-gauche* effect [26]. In solution, the chemical shift is an average over all the conformations. Some are in a *γ-gauche* conformation and induce upfield shifts up to 4 ppm. This averaging fades out in the solid, as the chain is locked in a particular conformation. In the nematic phase, the *gauche*-conformations involving the carbon atom directly bonded to the oxygen are statistically depleted, leading to a small effect on the chemical shift. However, in the solid, the packing arrangement may produce distorted valence bond angles which lead to the observed chemical shift differences [27]. In the nematic phase, the packing can play a similar role. For example, in PM4, the valence bond angles are slightly distorted: O36–C37–C38 (109·1(7)), C37–C38–C39 (111·9(7)), C38–C39–C40 (112·1(8)). In our compounds, the $-OCH_2-$ resonance of the side chain shows a noticeable upfield shift in the solid phase and a slight upfield shift in the nematic phase by comparison with the isotropic chemical shift. The *γ-gauche* effect cannot explain this behaviour [3]. In fact, the opposite temperature dependence of the $-OCH_2-$ resonance for the PM4 and PM4- chain-tilted compounds may be due to change in some valence bond angles within the lateral chain. At the solid–solid transition of PM4, the downfield shift may be a combination of the two factors. In the nematic phase, an upfield shift is observed by comparison with the isotropic chemical shift. However, the lack of the lateral methyl group gives a downfield shift [3]. This methyl group may therefore enforce the occurrence of sterically favourable conformations, leading to a larger proportion of *γ-gauche*-conformations in the nematic phase than in solution.

4. Conclusion

In this paper, we have presented the synthesis and properties of a new series of compounds containing four rings in the main core, and a lateral methyl group and a lateral alkoxy group on the same side of an inner ring. These compounds have large enantiotropic nematic phase ranges and, for the first members of the series, exhibit a solid–solid phase transition. The crystal

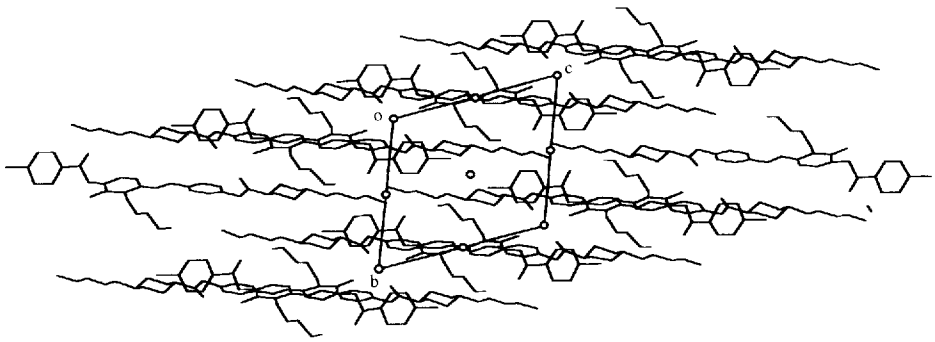

Figure 5. Projection of the PM4 structure along the *a* axis.

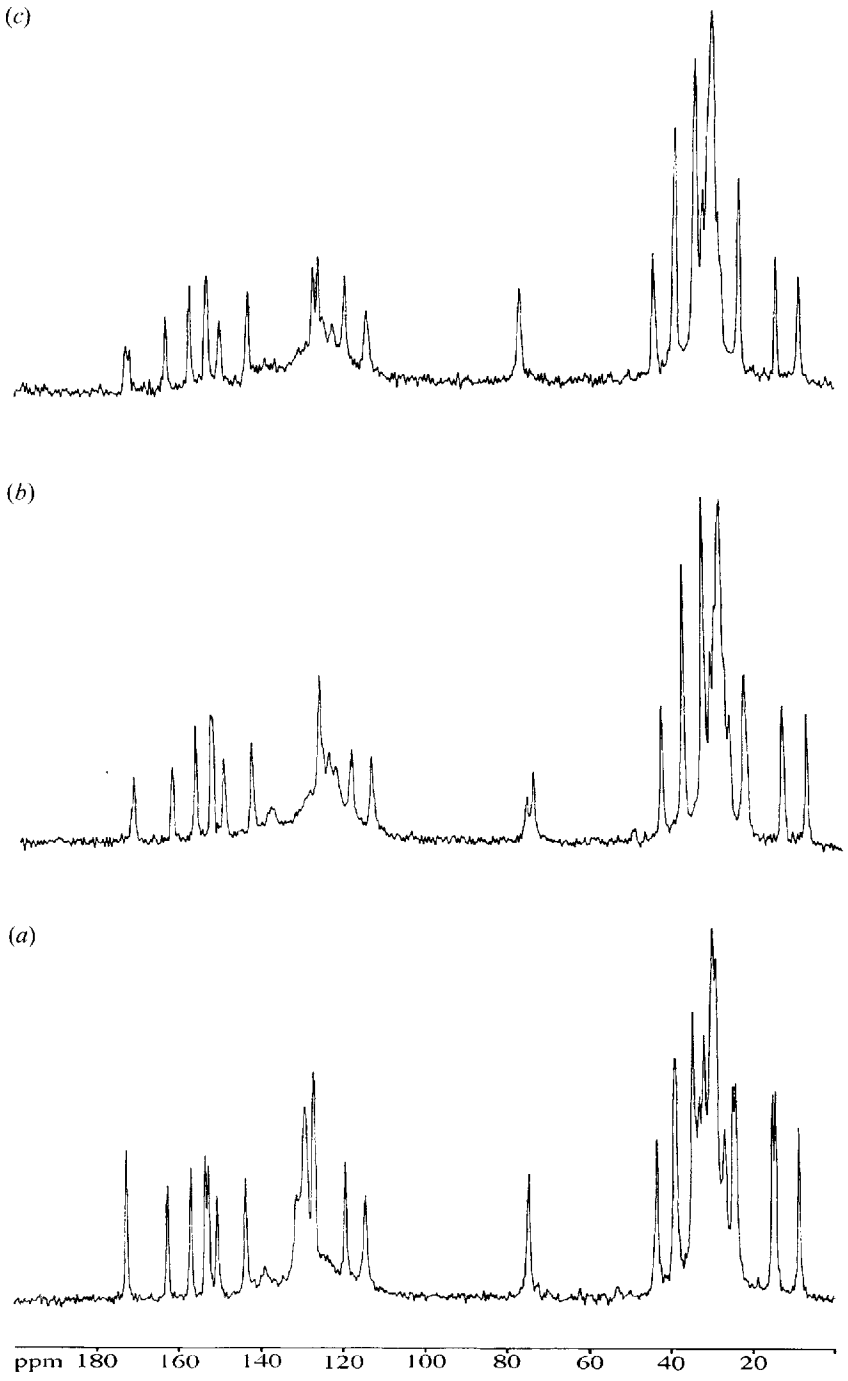

Figure 6. 50 MHz proton dipolar decoupled ^{13}C MAS NMR spectra of PM6: (*a*) below the solid-solid transition; (*b*) at the solid–solid transition; (*c*) above the solid–solid transition.

structures of two related compounds having the same side chain and a different end group indicate that the lateral chain can be obtained in different conformations. To probe the side chain conformation, we used the $-OCH_2-$ ^{13}C resonance of the side chain in the solid and nematic phases; a large downfield shift is observed for this resonance between the room temperature solid and the nematic phase. At the solid–solid phase transition, a similar downfield shift is observed which is associated with a tilt of the side chain. For the last members of the series, the solid–solid transition disappears due to the side chain interactions with the mesogenic cores of nearby molecules and the chain tilt occurs at the solid–nematic transition temperature. Other X-ray results on molecules with two lateral alkoxy chains will be published separately.

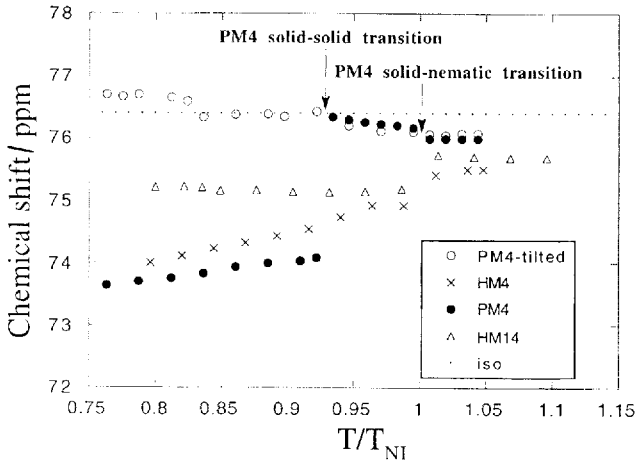

Figure 7. Chemical shift dependence of the lateral OCH_2 carbons in the HM4, HM14, PM4 and PM4-chain-tilted compounds on temperature. The straight dotted line indicates the mean isotropic chemical shift of these carbons obtained using $CDCl_3$ solutions.

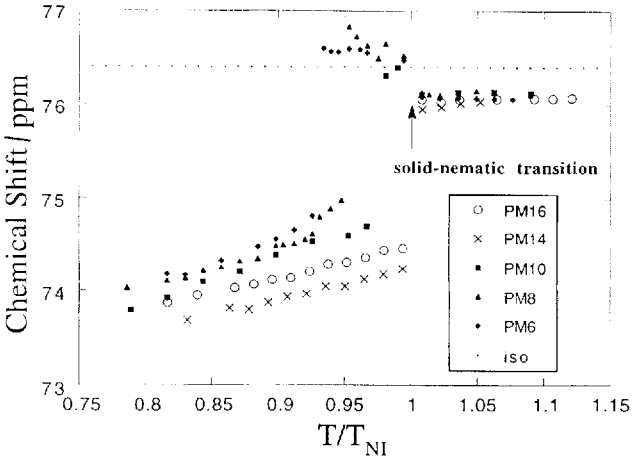

Figure 8. Chemical shift dependence of the lateral OCH_2 carbons in the PM6, PM8, PM10 and PM16 compounds on temperature.

References

[1] Perez, F., Judeinstein, P., Bayle, J. P., 1995, *New J. Chem.*, **19,** 1015.

[2] Berdagué, P., Perez, F., Bayle, J. P., Ho, Mei-Sing, and Fung, B. M., 1995, *New J. Chem.*, **19,** 383.

[3] Perez, F., Berdagué, P., Judeinstein, P., Bayle, J. P., Allouchi, H., Chasseau, D., Cotrait, M., and Lafontaine, E., 1995, *Liq. Cryst.*, **19,** 345.

[4] Weissflog, W., and Demus, D., 1985, *Mol. Cryst. liq. Cryst.*, **129,** 235.

[5] Demus, D., 1989, *Liq. Cryst.*, **5,** 75.

[6] Attard, G. S., and Imrie, C. T., 1989, *Liq. Cryst.*, **6,** 387.

[7] Nguyen, H. T., and Destrade, C., 1989, *Mol. Cryst. liq. Cryst. Lett.*, **6,** 123.

[8] Ballauf, M., 1987, *Liq. Cryst.*, **2,** 519.

[9] Imrie, C. T., and Taylor, L., 1989, *Liq. Cryst.*, **6,** 1.

[10] Hassner, A., and Alexanian, V., 1978, *Tetrahedron Lett.*, **46,** 4475.

[11] Nose, A., and Kudo, T., 1981, *Chem. Pharm. Bull.*, **29,** 1159.

[12] Berdagué, P., Perez, F., Courtieu, J., and Bayle, J. P., 1993, *Bull. Soc. Chim. Fr.*, **130,** 475.

[13] Lesot, P., Perez, F., Judeinstein, P., Bayle, J. P., Allouchi, H., and Cotrait, M., 1996, *J. Chem. Phys.* (submitted).

[14] Sheldrick, G. M., 1976, *SHELX76, Program for Crystal Structure Determination*, University of Cambridge, England.

[15] Gilmore, C. J., 1984, *J. appl. Cryst.*, **17,** 42.

[16] Lehman, H. S., Koetsel, T. F., and Hamilton, W. C., 1972, *J. Am. chem. Soc.*, **94,** 2657.

[17] Haw, J. F., 1988, *Anal. Chem.*, **559A,** 60.

[18] Akutagawa, T., Hoshino, N., Matsuda, I., and Matsunaga, Y., 1992, *Mol. Cryst. liq. Cryst.*, **214,** 117.

[19] Young, W. R., Haller, I., and Green, D. C., 1972, *J. org. Chem.*, **37,** 3707.

[20] Davies, K., 1983, *SNOOPI, Program for Drawing Crystal and Molecular Diagrams*, Chemical Laboratory, University of Oxford, England.

[21] Oulyadi, H., Lauprêtre, F., Monnerie, L., Mauzac, M., Richard, H., and Gasparoux, H., 1990, *Macromolecules*, **23,** 1965.

[22] Kato, T., Kabir, M. A., and Uryu, T., 1989, *J. Polym Sci. A*, **27,** 1147.

[23] Kato, T., Fujishima, A., Uryu, T., Matsushita, N., and Yamaguchi, H., 1990, *New Polym. Mater.*, **2,** 255.

[24] Kato, T., and Uryu, T., 1987, *Mol. Cryst. liq. Cryst. Lett.*, **5,** 17.

[25] Kato, T., and Uryu, T., 1991, *Mol. Cryst. liq. Cryst. Lett.*, **195,** 1.

[26] Tonelli, A. E., and Schilling, F. C., 1981, *Acc. chem. Res.*, **14,** 233.

[27] Tonelli, A. E., 1991, *Macromolecules*, **24,** 3605.